Chemistry, Physics and Technology of Surface. 2023. V. 14. N 4. P. 519-533

UDC 549.67+622.276.63+622.78 doi: 10.15407/hftp14.04.519

V.G. Tsitsishvili [1], N.M. Dolaberidze [2], M.O. Nijaradze [2], N.A. Mirdzveli [2], Z.S. Amiridze [2], B.T. Khutsishvili [2]

ACID AND THERMAL TREATMENT OF NATURAL HEULANDITE

[1] Georgian National Academy of Sciences
52 Rustaveli Avenue, Tbilisi, 0108, Georgia, E-mail: v.tsitsishvili@gmail.com
[2] Petre Melikishvili Institute of Physical and Organic Chemistry, Tbilisi State University
31 A. Politkovskaia Str., Tbilisi, 0186, Georgia

Acid treatment of natural zeolites is considered to be an effective method of "improving" their structure and properties, among which thermal stability occupies a special place, especially for catalytic applications of zeolites. The influence of hydrochloric acid solutions with concentrations up to 2 mol/L and calcination at temperatures up to 1100 °C on the structure and properties of heulandite-containing tuff from the Georgian Dzegvi-Tedzami deposit, selected for the creation of new bactericidal zeolite filter materials for purification and desinfection of water from various sources, was studied by the X-ray energy dispersion spectra, diffraction patterns and thermal analysis, as well as by adsorption of water, benzene and nitrogen methods. It has been found that an acidic environment leads to significant dealumination (Si/Al molar ratio increases from 3.6 to 9.5) and decationization (total charge of metal ions per Al atom decreases from 1 to 0.68) of the sample; solutions of hydrochloric acid do not lead to amorphization of the zeolite microporous crystal structure, but gradually dissolve it. As a result of acid treatment, there is also a sharp increase in the volume of micropores available for large molecules (from ≈ 7 to 80–90 mm^3/g) and surface area (from ≈ 13 to 120–175 m^2/g), as well as changes in the mesoporous system, leading to the prevalence of pores with a diameter of up to 4 nm. Heulandite heating leads to stepwise dehydration proceeding up to ≈ 800 °C, amorphization starting at ≈ 250 °C, and structural changes: the transition to methastable heulandite B phase at ≈ 340 °C is not fixed, but at ≈ 500 °C wairakite ($Ca(Al_2Si_4O_{12})\cdot 2H_2O$) is formed, at temperatures above ≈ 1000 °C, amorphous aluminosilicate contains crystalline inclusions of cristobalite (polymorph of SiO_2), α-quartz, albite ($Na(AlSi_3O_8)$, hematite (Fe_2O_3) and magnetite ($FeO\cdot Fe_2O_3$); heating-induced changes in micro- and mesopore systems are insignificant. It is also shown that heat treatment increases the acid resistance of heulandite, which is expressed in a decrease in the degree of dealumination after acid treatment of calcined samples. Thus, acid and heat treatment of heulandite make it possible to obtain materials with different sorption and ion-exchange properties.

***Keywords**: heulandite, dealumination, decationization, dehydration, amorphization*

INTRODUCTION

Natural and synthetic zeolites, hydrated microporous crystalline aluminosilicates of the general formula $M_x[Al_xSi_yO_{2(x+y)}]\cdot mH_2O$ (M^+ = Na^+, K^+, … $½Ca^{2+}$, $½Mg^{2+}$, ...), have a wide application due to unique set of molecular-sieve, sorption, ion exchange and catalytic properties [1]. In general, synthetic zeolites are more suitable for use as adsorbents (in particular, for the sequestration of heavy metals in wastewater treatment) due to the high uniformity of pore size distribution and the presence of a single compensation cation, while natural varieties, although very attractive from an economic and environmental points of view, demonstrate a lower sorption capacity (including that with respect to most heavy metals [2]). The problem is related to the porous crystalline structure of zeolites, built from alternating SiO_4 and AlO_4^- tetrahedra, forming open framework uniform structures with cages and channels, and to improve the performance of the zeolite, its structure can be changed by neat or chemical treatment. For example, acid treatment makes it possible to increase the surface area of the adsorbent and the effective porosity of the original natural zeolites [2–4], since exchangeable cations M^+ located in channels and cavities throughout the zeolite structure sometimes block the channel system [5]. However, concentrated acid solutions at high processing temperatures can cause significant aluminum leaching (dealumination with formation of a hydroxyl nest according to the reaction $Al(Si–O^-) + H_3O^+ + 3HCl \rightarrow 4(OH–Si–O) + Al^{3+} + 3Cl^- + H_2O$) and even destruction of the zeolite crystal structure.

Thus, the advantage of acid treatment is the removal of cations, which occupy a significant space in the micropores of zeolites, as well as other impurities, resulting in the development of new pores and active sites; the disadvantage of acid treatment, which occurs at a high concentration of acid, is dealumination, which can cause partial or complete destruction of the zeolite framework. As has been shown [6], hydrochloric and nitric acids are more efficient dealuminating agents than sulfuric and phosphoric acids, not to mention weak organic acids. The most widely used is hydrochloric acid, its effect on the structure and properties of zeolites is well studied for clinoptilolite rich natural zeolites [7, 8].

On the other hand, heat treatment is also used to improve the properties of natural zeolites [4]. The crystal structure of zeolites $M[AlSi_xO_{2(1+x)}]\cdot nH_2O$) includes three components: an aluminosilicate framework $[AlSi_xO_{2(1+x)}]$, cations M^+ that compensate for its negative charge, and water molecules. When the zeolite is heated, water molecules gradually leave the crystal lattice, cations change their positions, which can lead to changes in the structure of the aluminosilicate framework. The stability of the zeolite framework plays an important role, and it can be assumed that preliminary heat treatment can affect the acid resistance of the sample.

The purpose of this paper is to consider changes in the structure and properties of heulandite-containing tuff from the Tedzami-Dzegvi deposit (Eastern Georgia) under influence of acid and thermal treatment based on new and previously published data on characterization [9], dehydration and structural transformations [10], acid [11, 12] and thermal [13] treatment, as well as on acid resistance and ion-exchange capacity [14] of this natural zeolite selected as a raw material to create new bactericidal zeolite filter materials for purification and desinfection of water from various sources.

EXPERIMENTAL

Materials. Samples of heulandite-containing tuff were collected in the southern section of the Tedzami-Dzegvi deposit, Eastern Georgia. According to the results of recent study [9], the sample contains up to ≈ 90 % of zeolite phase consisting of high-silica heulandite mixed with chabazite in a ratio of 8:1. Zeolitic tuff was crushed on a standard crusher, fractionated to a particle size of 1–1.4 mm (14–16 mesh), washed with distilled water to remove clay impurities, and dried at a temperature of 95–100 °C.

Treatment. Acid treatment of samples was carried out by mixing 10 g of sieved, washed and dried original zeolitic tuff with 100 ml of 0.5, 1.0, and 2.0 mol/L HCl solutions in a shaking water bath (OLS26 Aqua Pro, Grant Instruments, US) operating in linear mode at 75 °C. To achieve maximum effect, acid treatment was carried out in three steps: the first lasted 1 hour, the second – 2 hours, and the third – 3 hours, each step was followed by washing with distilled water until no Cl^- ions were detected in the washing water by using $AgNO_3$ solution. The washed and dried samples were weighed to determine the weight loss (see Table 1).

Table 1. Weight loss (%) from acid treatment steps

Step	Concentration of HCl solution (mol/L)		
	0.5	1.0	2.0
1st	9.75	12.8	15.4
2nd	7.05	7.8	7.95
3rd	4.5	6.1	5.25

Calcination of prepared samples in the temperature range of 200–1100 °C was carried out in a muffle furnace B400/410 (Naberthem, Carl Stuart Group). Zeolite samples were placed in a muffle furnace in heat-resistant round-bottom cups, subjected to heat treatment under static conditions for 1 hour, and then, after a while, these cups were placed in desiccators with calcined $CaCl_2$ until complete cooling.

Characterization. Chemical composition of samples was calculated from the X-ray energy dispersive (XR-ED) spectra obtained from a scanning electron microscope JSM-6490LV (Jeol, Japan) equipped with an INCA Energy 350 XRED analyzer (Oxford, UK). Powder X-ray diffraction (XRD) patterns were obtained from a D8 Endeavor diffractometer (Bruker, Germany) and a modernized Dron-4 (USSR) diffractometer both employing the CuK_α line (λ = 0.154056 nm); the samples were scanned in the 2Θ range of 5° to 68° with a 0.02° step at a scanning speed of 1°/min. Thermogravimetric analysis was based on weight loss (TG), difference thermal analysis (DTA) and difference thermogravimetric (DTG) curves recorded on an STA 2500 Regulus thermal analyzer (NETZSCH group) at the heating rate of

10ºC/min. The adsorption capacity for water and benzene vapors was measured under static conditions at room temperature; samples calcined at 260–280 °C and then weighed on an electronic analytical balance (FA 2204N, JOAN LAB, China) were placed in a desiccator and kept for 96 hours at a constant pressure of water vapor (relative pressure p/p_o = 0.4 and saturated vapor pressure p/p_o = 1.0) and benzene (p/p_o = 1.0) and then the samples that absorbed the vapors were weighed again. Nitrogen adsorption/desorption isotherms were measured at 77 K using an ASAP 2020 Plus analyzer (Micromeritics, USA) on samples vacuum degassed at 350 °C, data analysis was carried out using Brunauer–Emmett–Teller (BET) and Barrett-Joyner-Halenda (BJH) models.

RESULTS AND DISCUSSION

Chemical composition. The results for chemical composition of the acid-treated samples calculated for 72 oxygen atoms in the unit cell are given in Table 2 in terms of averaged empirical formulas of dehydrated zeolites; the Si/Al molar ratio shows the degree of dealumination.

An increase in the Si/Al molar ratio by more than two and half times indicates a rather high degree of acid-mediated dealumination. Dealumination of acid-treated samples limits their use as ion exchangers due to a significant reduction in cation-exchange capacity (CEC), calculated from XR-EDS data as the number of milliequivalents of ionogenic groups per gram of the ion exchanger fully converted to the H^+ form (see Fig. 1).

The degree of decationization is shown in Fig. 2 by a decrease in the total charge of the compensating ions Na^+, K+, Ca^{2+} and Mg^{2+}, as well as the share of each of these cations in compensating the negative charge of the zeolite framework as they are leached and replaced in the framework by H^+.

The total charge of metal cations per one aluminum atom monotonically decreases from ≈ 1 to ≈ 0.68 with increasing acid concentration. The contribution of Na^+ ions to compensate for the negative charge on aluminum atoms decreases, so that sodium is leached to the greatest extent (its content decreased ≈ 9 times after treatment with 2.0 mol/L solution); Mg^{2+} ions are washed out to a lesser extent, the content of Ca^{2+} ions decreased slightly (–7 %), and K^+ ions do not take part in the decationization process. This conclusion is consistent with the results of the study of decationization and dealumination of clinoptilolite tuff [7] where was also found that natural clinoptilolite samples treated with HCl solutions exchanged mainly Na^+ ions, followed by $Mg^{2+}$and Ca^{2+} ions, whereas K^+ ions from the clinoptilolite practically did not participate in an exchange process. However, our results do not correspond to the data of work [8] that the removal of monovalent cations, such as Na^+ and K^+ ions, is insignificant for the temperatures of 25–100 °C and changed little with acid concentration, but the results are difficult to compare, since high-silica clinoptilolite (Si/Al = 6.22) was used in the study of Turkish scientists.

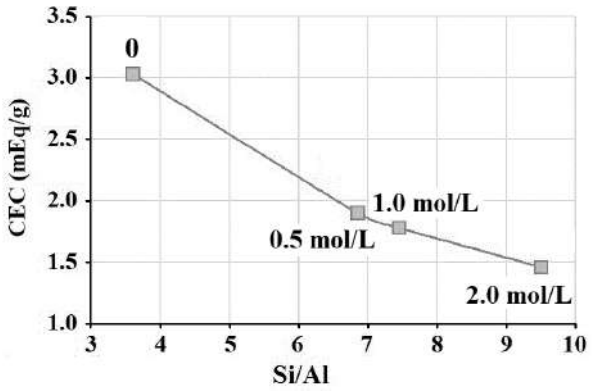

Fig. 1. Dependence of CEC on the Si/Al molar ratio of original (0) and acid-treated samples

Table 2. Chemical composition of original and acid-treated samples

Concentration of HCl solution (mol/L)	Empirical formula	Si/Al
0	$(Na_{1.96}K_{0.47}Ca_{1.49}Mg_{1.17})[Al_{7.8}Si_{28.2}O_{72}]$	3.6
0.5	$(Na_{0.62}K_{0.67}Ca_{0.71}Mg_{0.47})[Al_{4.59}Si_{31.4}O_{72}]$	6.85
1.0	$(Na_{0.47}K_{0.40}Ca_{0.65}Mg_{0.46})[Al_{4.26}Si_{31.7}O_{72}]$	7.45
2.0	$(Na_{0.096}K_{0.50}Ca_{0.61}Mg_{0.26})[Al_{3.43}Si_{32.6}O_{72}]$	9.5

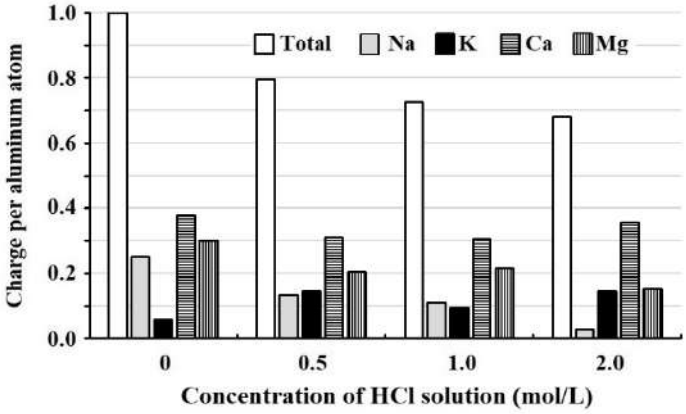

Fig. 2. Cationic charge per Al atom of native (0) and acid-treated samples

Table 3. Chemical composition of original and heat-treated samples

Calcination temperature (ºC)	100	200	400	500	600	700	800
Si/Al	3.60	3.68	3.72	4.26	3.77	3.67	3.72
Na/Al	0.25	0.26	0.26	0.26	0.27	0.26	0.25
K/Al	0.06	0.07	0.06	0.07	0.07	0.06	0.07
Ca/Al	0.19	0.195	0.19	0.195	0.20	0.19	0.19
Mg/Al	0.15	0.145	0.15	0.155	0.15	0.14	0.15
[Na+K+2(Ca+Mg)]/Al	0.99	1.01	1.00	1.04	1.06	0.98	1.00

According to the XR-ED spectra, chemical composition of the surface of the calcined samples undergoes slight changes, which are most reflected in the Si/Al molar ratio (see Table 3) – after annealing at the temperature of 500 °C, dealumination is observed; at higher temperatures, the modulus Si/Al returns to its previous values.

The data presented in Table 3 indicate that, as a result of heating, decationization of heulandite does not occur, the negative charge of the framework is completely compensated by sodium, potassium, calcium and magnesium cations.

Structure. Powder XRD patterns show no changes after treatment with a dilute HCl solution (0.5 mol/L), but treatment with concentrated solutions leads to a change in the intensity of some peaks (see Fig. 3, left).

Thus, the intensity of the low angle peak at 2Θ = 9.85° (Miller indices *hkl* 020; *d*-spacing 8.98 Å) decreases with increasing acid concentration, the peak intensities at ≈ 22° (*hkl* 131, 400, 330; ≈ 4 Å) first increase (at acid concentration 1.0 mol/L), and then decrease (2.0 mol/L), while the intensity of the weak peak at ≈ 28° (*hkl* −422 and/or −441; ≈ 3.15 Å) initially decreased and then sharply increases with increasing acid concentration to 2 mol/L. In addition, some peaks decrease and disappear from X-ray diffraction patterns with increasing acid concentration, this applies to peaks at 2Θ = 13° (*hkl* −201; 6.8 Å), 15° (*hkl* 220; ≈ 6 Å) and ≈33° (*hkl* -261 and/or 061; ≈ 2.8 Å).

No line broadening is observed, so that the acid treatment does not cause amorphization of the sample. The overall intensity of the XRD pattern decreases slightly with increasing acid

concentration, not correlating with the much greater weight loss resulting from the treatment shown in Table 1. Although the chemical composition of the zeolites does not change in the third step of the acid treatment, there is still a slight weight loss, which indicates the gradual dissolution of the samples by the acid.

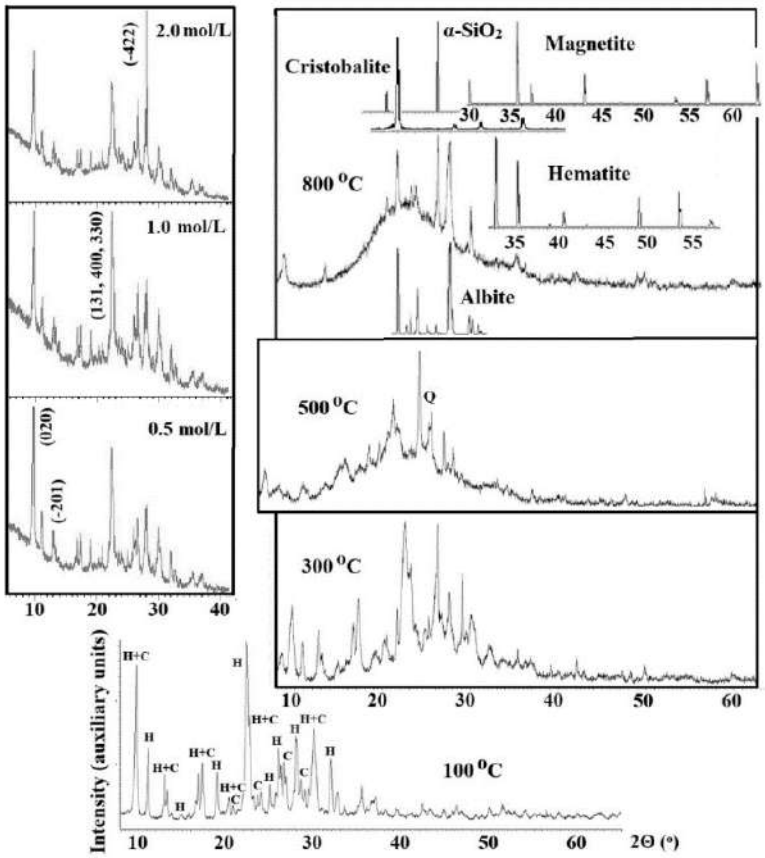

Fig. 3. Powder XRD patterns of dried at 100 °C sample (bottom, H – peaks of main heulandite phase, C – peaks of impurity chabazite phase), acid treated samples (left, numbers in parenthesis are Miller indices *hkl* of peaks changing intensity) and samples calcined at 300, 500 and 800 °C (right)

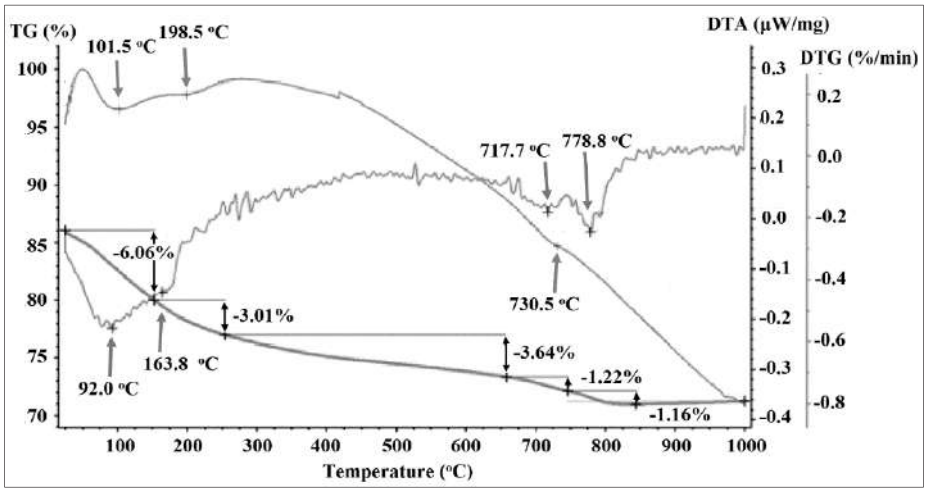

Fig. 4. Thermogravimetric curves of heulandite (red and blue arrows show endothermic peaks on DTA and DTG curve, respectively)

The result obtained does not contradict the known ones, since in a recent work [6], the amorphization of clinoptilolite recorded using XRD patterns was noted only after treatment of the zeolite with solutions with a high concentration of hydrochloric acid (5 and 10 mol/L).

XRD patterns do not change in the temperature range up to 200 °C, at higher temperatures the peaks begin to broaden, than the intensity of the heulandite peaks decreases, and at ≈ 500 °C a broad band and a sharp peak of quartz (2Θ = 26.6°) appear (Fig. 3, right).

Thermogravimetric curves (Fig. 4) show slow endothermic peaks at relatively low temperatures (DTA at 101.5 and 198.5 °C, DTG at 92.0 and 163.7 °C), but no sharp endothermic peak at ≈ 340 °C, which is associated with the transition to the structure of "sluggish" [15] heulandite B, first described by Koizumi [16]. Probably, the absence of a transition to heulandite B is explained by the lower aluminum content in Georgian heulandite (Si/Al = 3.6) than that in the low-silica samples studied in works [15–17].

It is believed that when heulandite is heated, the metastable phase of heulandite B exists in the temperature range of 340–470 °C, and at temperatures exceeding 500 °C a mixture of quartz (SiO_2) and minerals of the 9.GB.05 group such as wairakite ($Ca(Al_2Si_4O_{12})\cdot 2H_2O$) and/or anorthite ($Ca(Al_2Si_2O_8)$) starts to appear. The XRD patterns cannot unequivocally confirm the formation of these minerals, since the most intense peaks for wairakite and anorthite (2Θ ≈ 16 and 28°, respectively) overlap with the peaks of chabazite (reflection with *hkl* = 113 giving an intense peak at 2Θ = 16° [18]) and heulandite ((*hkl* = -422 at 2Θ = 28.1°, and *hkl* = -441 at 2Θ = 28.5°). However, the formation of wairakite containing "zeolite water" is confirmed by thermal analysis data: the measured total weight loss (15.09 %) is in good agreement with the calculated one (15.5 %) for 3 water molecules per aluminum atom, most of the water (≈ 6 % of the total weight loss or ≈ 60 % of the total water content) is continuously lost at temperatures below ≈ 250 °C, and then part of the remainder (≈ 24 % of the total water content) is slowly dehydrated up to 650 °C, complete dehydration of the sample is achieved at ≈ 800 °C; high-temperature endothermic peaks are registered on the DTA curve at 730.5 °C, on the DTG curve at 717.7 and 778.8 °C.

Apparently, these endothermic effects are associated with the formation of new crystalline phases – the silica polymorph cristobalite, which gives an intense peak at 2Θ = 26.6° in the XRD pattern, and sodium feldspar albite ($NaAlSi_3O_8$), which gives intense peaks in a range of 2Θ = 22–32°. In the powder XRD pattern of the Dzegvi-Tedzami heulandite sample calcined at 800 °C (Fig. 3, right, top), low-angle broadened peak of chabazite is visible at 2Θ = 9.4° (Miller indices *hkl* 100; *d*-spacing 9.4 Å), but the main part of the amorphized zeolite phase is represented by a wide band at 2Θ from 12 to 40° superimposed by narrow lines of silica, cristobalite and albite peaks. It should be noted that the XRD pattern of calcium feldspar anorthite ($Ca(Al_2Si_2O_8)$) is characterized by an intense peak at 2Θ ≈ 28°, the XRD pattern of potassium feldspar orthoclase ($K(AlSi_3O_8)$) shows peaks in a range 2Θ = 20–35°, and these peaks may be overlapped by albite peaks, although the formation of orthoclase is unlikely due to the relatively low content of potassium in the sample. In addition, peaks of impurity oxides of iron, hematite (Fe_2O_3, peaks in a range of 2Θ = 33–60°), and magnetite ($FeO\cdot Fe_2O_3$, peaks in a range of 2Θ = 30–65°) appear in the pattern after calcination at high temperatures.

Complete amorphization of all zeolite phases (heulandite, wairakite, and chabazite) is achieved after calcination at 1000 °C; at higher temperatures, the amorphous aluminosilicate contains crystalline inclusions of cristobalite, α-quartz, albite (and possibly also anorthite), hematite and magnetite (see Fig. 5).

With an increase in the calcination temperature, the intensity of the quartz peak decreases, and the intensity of the cristobalite peak sharply increases, the feldspar (albite and possibly anorthite) peaks are preserved up to 1100 °C, and the peaks of iron oxides become more distinct. Hematite melts at 1565 °C, magnetite begins to decompose at 1950 °C [19], and in the XRD patterns of sample calcined at high temperature (1200–1300 °C), the ratio of the intensity of the peak at 2Θ = 35.8°, consisting of the peaks of magnetite (75 %) and hematite (x), to the intensity of the magnetite peak at 2Θ = 33.2° (100 %) is approximately 2:1, which allows us to estimate the relative content of hematite (x) as 125 % of the content of magnetite.

Adsorption of water and benzene. Water molecules have a small kinetic diameter of 0.266 nm and can freely pass through entrance windows into heulandite channels, and the adsorption of water vapor at a relative pressure p/p_o = 0.4, corresponding to almost complete filling of micropores, is a measure of their volume available for small polar molecules [20], while adsorption at saturated water vapor pressure ($p/p_o \approx 1$) is a measure of the total pore volume. The kinetic diameter of the benzene molecule (0.585 nm) significantly exceeds the sizes of micropores and channels, so that this non-polar molecule can be adsorbed only on the zeolite surface developed due to the presence of meso- and macropores; benzene adsorption capacity is a relative measure of surface area and its hydrophobicity. Results of measurements are shown in Fig. 6.

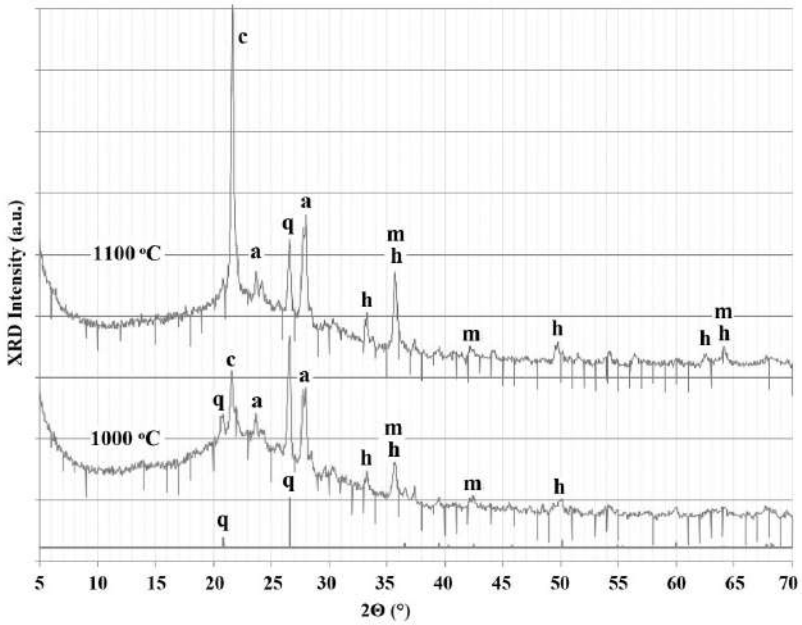

Fig. 5. Assignment of peaks in powder XRD patterns of the Dzegvi-Tedzami heulandite sample calcined at 1000 and 1100 °C: q – α-SiO_2, c – cristobalite, a – albite and anorthite, h – hematite, m – magnetite

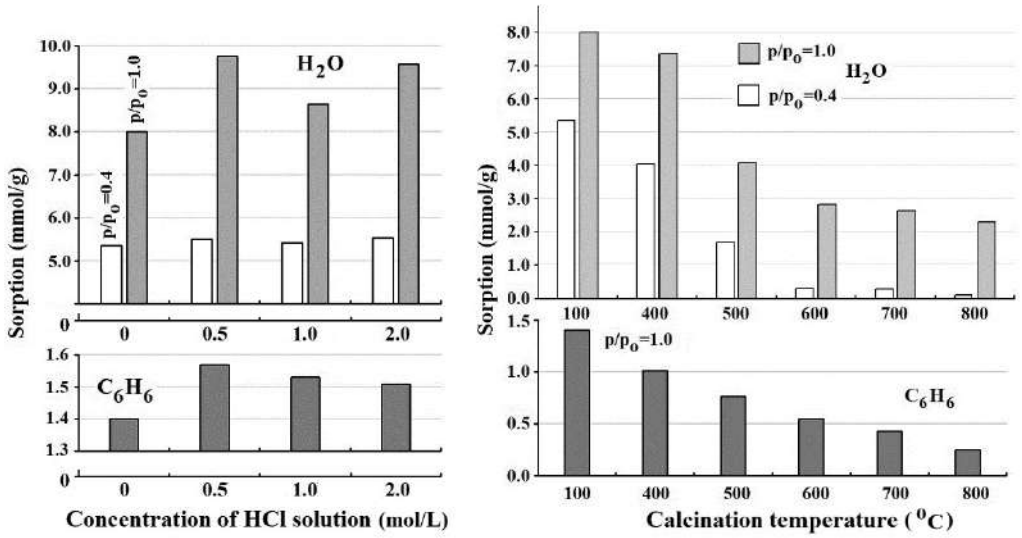

Fig. 6. Water vapor (H_2O) and benzene (C_6H_6) adsorption capacity of acid-treated (left) and calcined (right) samples

The volume of micropores accessible for water molecules in native heulandite is about 60 % of the total pore volume. Adsorption in micropores practically does not change as a result of acid treatment and decreases with an increase in the calcination temperature, reaching very low values (< 0.3 mmol/g) at temperatures above 500 °C; it is in no way related to the aluminum content, as was noted in studies of water vapor adsorption on high-silica synthetic zeolites reviewed in [20]. The adsorption capacity of all pores with respect to water vapor in acid treated samples changes nonmonotonically and decreases with an increase in the calcination temperature.

The adsorption of benzene vapor after treatment with a solution of hydrochloric acid with a concentration of 0.5 mol/L increases, which clearly indicates an increase in the hydrophobicity of the surface, but with an increase in acid concentration, this effect is leveled; the heat treatment leads to decrease of hydrophobicity.

Adsorption of nitrogen. In heulandite crystal structure, a 10-membered ring (0.75×0.31 nm) and one of the 8-membered rings (0.47×0.28 nm) cannot accommodate a nitrogen molecule (kinetic diameter 0.364 nm), which can pass only into one 8-membered ring (0.46×0.36 nm). The low-temperature adsorption-desorption isotherms of nitrogen on studied native, acid-treated and calcined samples correspond to the filling of micropores (Langmuir plot) at low relative pressures (p/p_o < 0.3) and demonstrate a hysteresis loop with a jump at p/p_0 = 0.4–0.5 indicating the presence of developed system of mesopores (see Fig. 7).

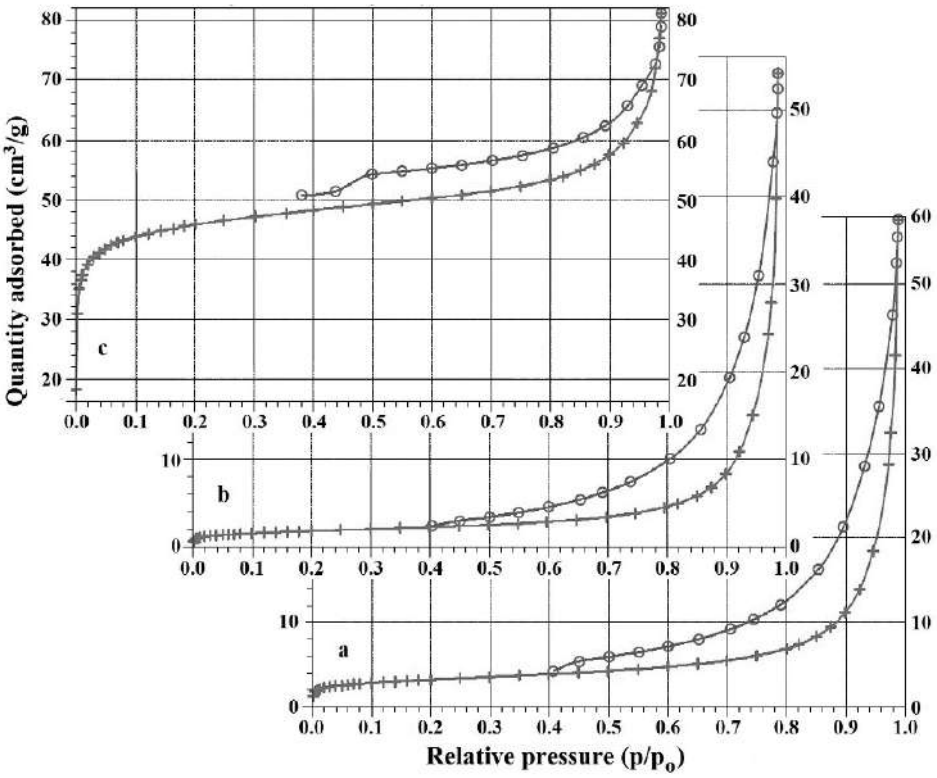

Fig. 7. N_2 adsorption-desorption isotherms on native Georgian heulandite (*a*) and its thermal treated (800 °C, *b*) and acid-treated (2.0 mol/L, *c*) samples

According to the so-called BDDT classification of isotherms [21] adopted by IUPAC, as well as the classification of hysteresis loops [22], the obtained isotherms belong to type IV (complete filling of pores) with a combined hysteresis loop: H_1 (cylindrical pore channels) in the region of high relative pressures and H_3 (slit-shaped pores) in the region medium pressures $0.4 < p/p_o < 0.9$.

The Brunauer-Emmett-Teller (BET [23]) model ideally describes the experimental data in the range of relative pressures $0.01 < p/p_o < 0.25$,

significant discrepancies between the BET equation ($\{W[(p/p_o) - 1]\}^{-1} = (W_mC)^{-1} + \{[(C - 1)/W_mC)]\ (p/p_o)\}$, where W is adsorption at pressure p, W_m is the monolayer volume on the adsorbent surface, C is the ratio of the adsorption equilibrium constant in the first layer and the condensation constant) occur at relative pressures $p/p_o > 0.5$ (see Fig. 8).

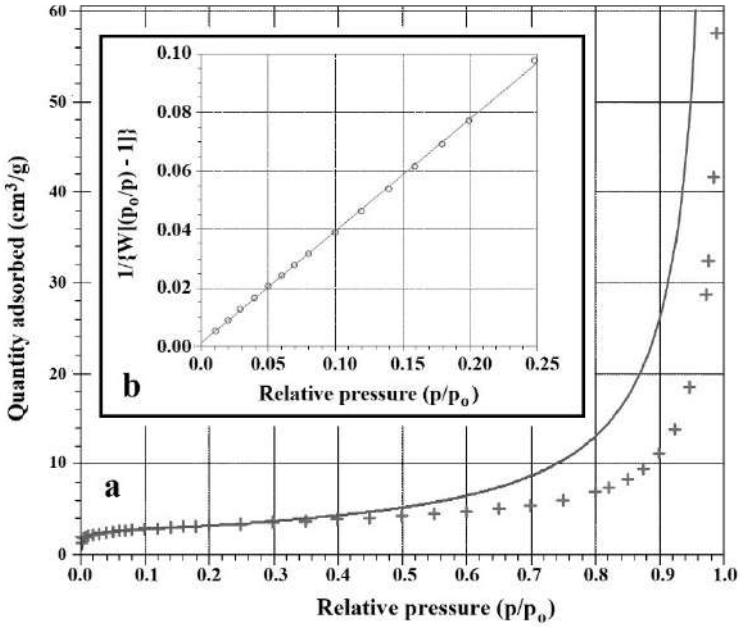

Fig. 8. BET isotherm plot (*a*, solid line – calculation according to the BET equation, crosses – measured values of adsorption) and BET surface area plot (*b*)

Table 4. Porosity parameters of initial, acid treated and calcined samples

Parameter	Initial	Concentration of HCl (mol/L)			Calcination temperature (°C)				
		0.5	1.0	2.0	400	500	600	700	800
S_{BET} (m^2/g)	12.8	127	155	175	11.4	10.5	9.45	9.16	6.52
$Q_{1.0}$ (cm^3/g)	57.89	48.8	55.8	68.1	57.64	60.0	53.14	50.40	54.16
$Q_{0.4}$ (cm^3/g)	4.184	35.0	42.3	48.2	3.879	3.668	3.286	3.207	2.258
V_p (mm^3/g)	89.5	109	113	126	89.2	92.8	82.2	78.0	83.8
V_m (mm^3/g)	6.47	78.2	85.6	88.9	6.0	5.7	5.1	5.0	3.5
D_{BJH} (nm)	17.2	13.1	11.6	11.1	17.6	17.6	17.2	16.1	20.1

The constant C for a native sample is 369 ± 64, for calcined samples C decreases to 170 ± 10, for acid-treated samples it varies within (1200–1400) ± 350, so that in any case $C >> 1$ and the BET equation can be simplified to $\{W[(p/p_o) - 1]\}^{-1} = [(p/p_o)/W_m]$. In this case, the constant C is no longer a parameter of the BET equation, the calculation of C from the slope **s** and the intercept **i** of the BET surface area plot (Fig. 6 *b*, C = s/i) is purely formal (i→0) and has no physical meaning.

Turkish researchers [6] processed data in the region of low relative pressures ($p/p_0 < 0.1$) using the Dubinin-Astakhov equation ($W = W_0\exp\{-[R\mathrm{T}\ln(p_0/p)/E]^n\}$, where W_0 is total weight adsorbed, E is the characteristic energy, R – gas constant, T – temperature) and obtained fractal values of the heterogeneity parameter n for acid-treated samples. In our case, there is no need to use the Dubinin-Astakhov or simplified Dubinin-Radushkevich (n = 2) equations, since the monolayer volume W_m can be determined with high accuracy (± 0.3–0.4 %) from the slope of the BET surface area plot, from which the surface area S_{BET} can be calculated using the formula $S_{BET} = W_mN_AA_x/M$, where N_A is Avogadro constant ($6.023\cdot10^{23}$ mol^{-1}), A_x – effective cross-

sectional area of N_2 molecule (0.162 nm^2), M – adsorptive (nitrogen gas) molar volume (22.414 mL/mol). The S_{BET} values and other porosity parameters calculated on the basis of experimental adsorption-desorption isotherms on initial, acid-treated and calcined samples are given in Table 4.

The total volume of pores V_p is calculated from the maximum quantity adsorbed $Q_{1.0}$, measured at saturated pressure of nitrogen gas; micropore volume V_m is calculated from $Q_{0.4}$, quantity adsorbed at relative pressure $p/p_o = 0.4$. Estimation of the mesopore size and calculation of the pore size distribution was carried out by the Barrett-Joyner-Halenda (BJH) method [24] using the Kelvin equation, which provides a correlation between the pore diameter and condensation pressure, so that the BJH desorption average pore diameter D_{BJH} is calculated as $D_{BJH} = 2(r_k + t)$, where the critical radius $r_k(Å) = 4.15/[\log(p_o/p)]$ for nitrogen desorption at 77 K, and the statistical thickness $t(Å) = 3.54[5/\log(p_o/p)]^{0.333}$, according to the Halsey equation [25] and Faass correction [26].

The initial sample has a low surface area (12.8 m^2/g), and the fraction of micropores accessible to nitrogen molecules is only 7 % of the total porosity. Under the influence of acid, the surface area and the volume of micropores accessible to nitrogen molecules increase sharply and continue to increase with increasing acid concentration in the treatment solution. A similar effect was noted in [6] for acid-treated clinoptilolite: (i) the volume of micropores accessible to nitrogen in the studied original clinoptilolite was only 0.005 cm^3/g, which the authors attributed to the blocking of most of the pores by cations considered as impurities; (ii) with an increase in the concentration of HCl in the solution, the volume of micropores increased by more than 12 times, up to 0.064 cm^3/g for 3 mol/L HCl solution but with further increase in the concentration, it decreased; (iii) the outer surface area of the HCl treated samples gradually increased with increasing the Si/Al ratio from 3 m^2/g and reached a maximum of 33 m^2/g after soaking in a 10 mol/L solution. Akimkhan [27] observed no increase in the total pore volume when clinoptilolite was treated at room temperature with 3 mol/L HCl solution for 24 hours, the increase was about 2 times when the concentration of acid was 12 mol/L, and over 3 times when the acid treatment was carried out at 96–98 °C.

According to the results obtained, the total pore volume V_p increases monotonically with increasing acid concentration, while the diameter of nanosized pores D_{BJH} sharply decreases. Silva and coworkers [28] found that HCl treatment decreased the zeolite pore diameter about 2.5 times and increased the surface area approximately 16 times.

Wide hysteresis loop of adsorption-desorption isotherms indicates broad pore size distribution, and the curve $V(D)$ (pore volume V vs. pore diameter D, see Fig. 9, left) calculated using BJH model from desorption isotherm measured on original heulandite sample shows the presence of mesopores up to 100 nm in diameter.

As the pore size distribution curves $V(D)$ of acid-treated samples show, the shape of the curve changes and the volume of mesopores decreases as a result of acid treatment. Thus, the observed slight increase in the total pore volume is mainly due to the "opening" of micropores for nitrogen molecules. According to the parameters given in Table 4, after processing the sample in solutions with a concentration of 0.5, 1.0 and 2.0 mol/L, the specific volume of micropores increases to 72, 716 and 71 % of the total pore volume, respectively.

Pore size distribution differential dV/dD vs. pore diameter curves (Fig. 9, right) show that the original heulandite is characterized by a wide size distribution of mesopores from 2 to 50 nm in diameter with a maximum at ≈ 12 nm; as a result of acid treatment, this maximum disappears, but a sharp maximum at ≈ 4 nm, which increases with increasing acid concentration, appears. Taking into account, albeit small, but still an increase in the total pore volume with increasing acid concentration, it can be concluded that after acid treatment, small in size, up to 4 nm, pores become predominant in the mesopore system of the acid-treated heulandite. These effects of acid treatment are most pronounced when using dilute solutions of hydrochloric acid (with a concentration of less than 0.5 mol/L), the pore size distribution curves for samples treated with 1 and 2 normal solutions practically do not differ.

Apparently, the described changed in the distribution of mesopore sizes also lead to the fact that the hysteresis loop for acid-treated samples does not "close" (see Fig. 7) at a relative pressure

p/p_o = 0.4, which is considered as a conditional boundary between adsorption in micropores and mesopores.

With regard to heat treatment, surface area S_{BET} decreases monotonically from 12.8 to 6.5 m^2/g (see Table 4) with an increase in the calcination temperature, the total volume of pores varies insignificantly, reaching a maximum value after calcination at 500 °C and a minimum after annealing at 700 °C, while the volume of micropores accessible to nitrogen molecules decreases insignificantly up to 700 °C (from 6 to 5 mm^3/g), and after annealing at 700 °C it drops sharply to 3.5 mm^3/g. Probably, the retention of such a low adsorption capacity up to high temperatures is due to the existence of a heat-resistant impurity phase of chabazite and the formation of microporous wairakite.

The average mesopore diameter D_{BJH} slightly changes as a result of calcination, and as the pore size distribution curves $V(D)$ (see Fig. 10) show, the volume of mesopores decreases, although the difference between the distribution of mesopores in samples calcined at 400 and 800 °C is insignificant. The nature of the pore size distribution (maximum at ≈ 12 nm) remains the same, and this is clearly seen in Fig. 11, which shows the differential pore size distribution curves dV/dD for heulandite calcined at different temperatures.

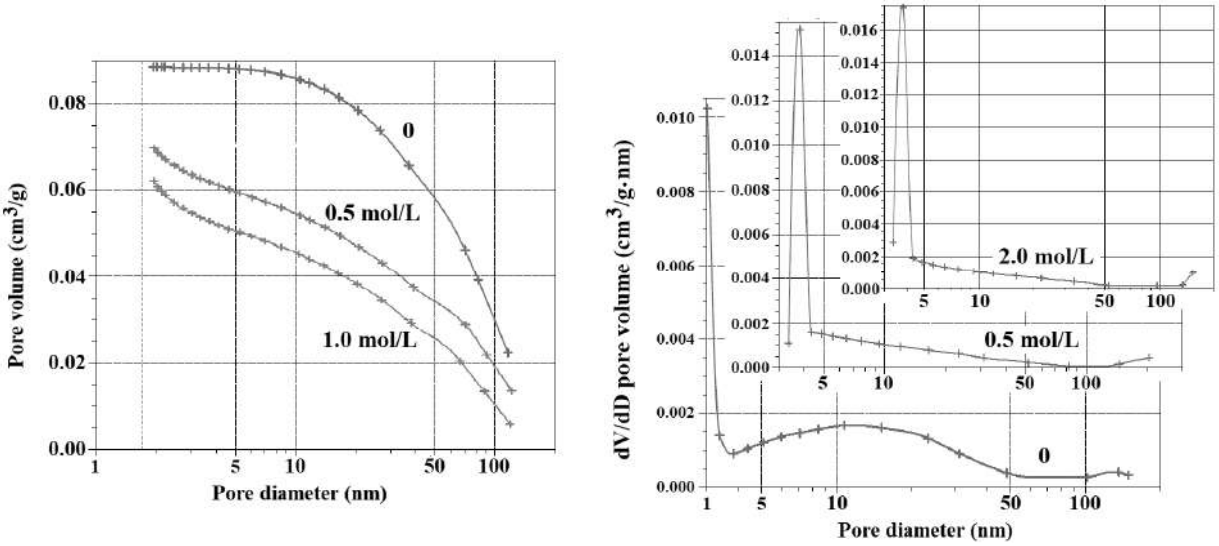

Fig. 9. Pore size distribution volume V vs. pore diameter D (left) and differential dV/dD vs. pore diameter (right) curves calculated by BJH model for original heulandite (0) and its acid-treated forms

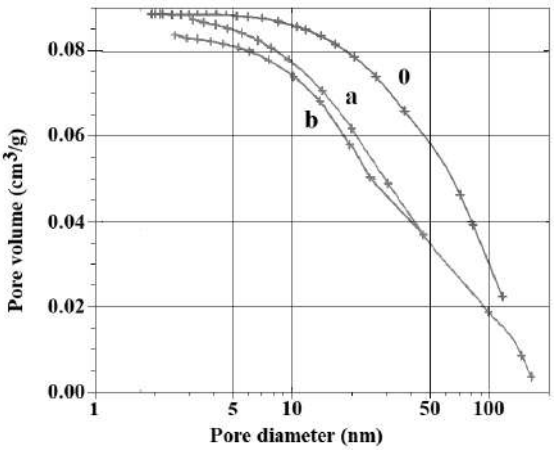

Fig. 10. Pore size distribution curve volume vs. pore diameter $V(D)$ calculated by BJH model for original (0) and calcined at 400 °C (*a*) and 800 °C (*b*) heulandite samples

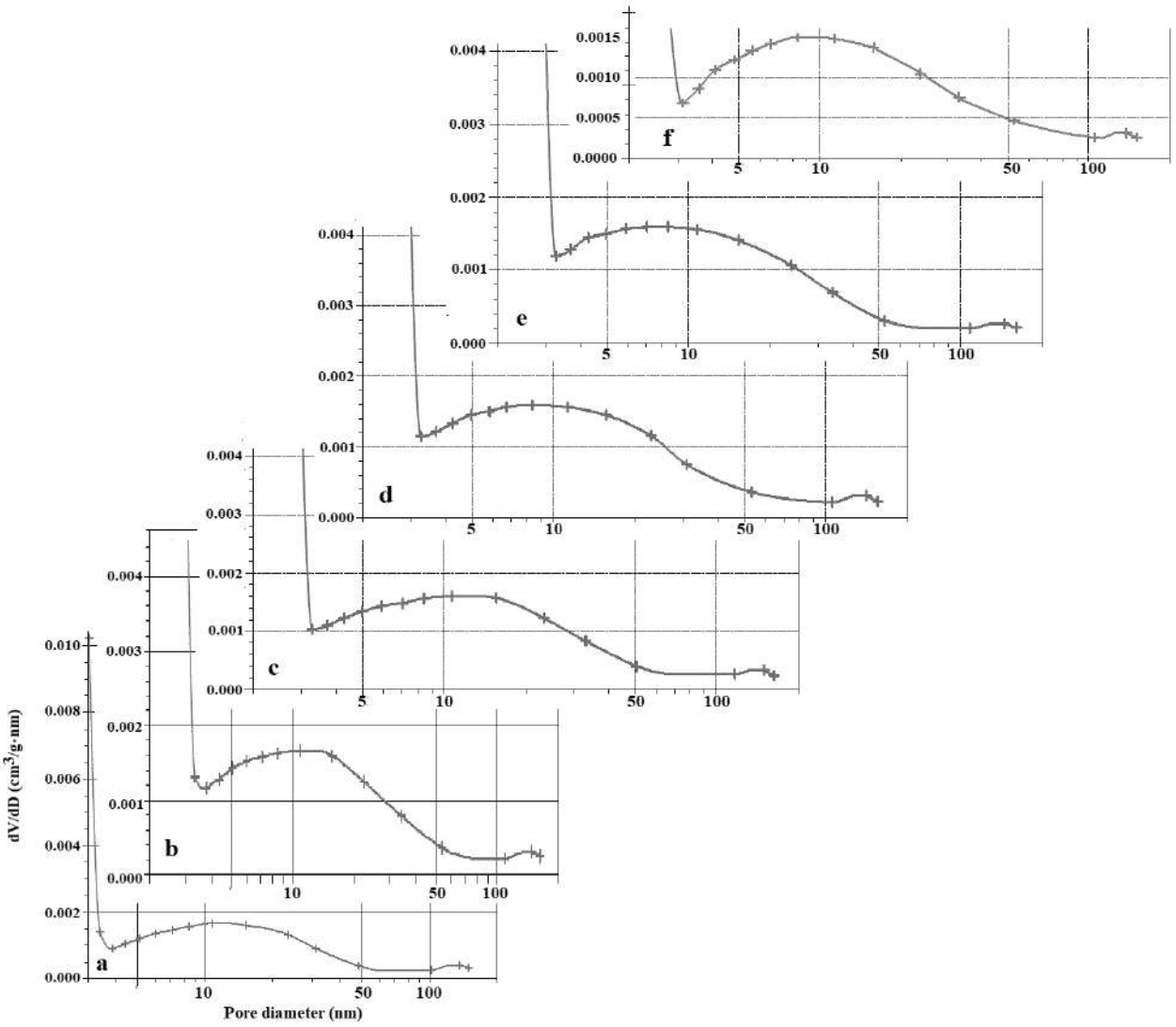

Fig. 11. Pore size distribution d*V*/d*D* curves calculated on the basis of the BJH model from desorption isotherms measured on Georgian heulandite calcined at 100 (*a*), 400 (*b*), 500 (*c*), 600 (*d*), 700 (*e*) and 800 °C(*f*)

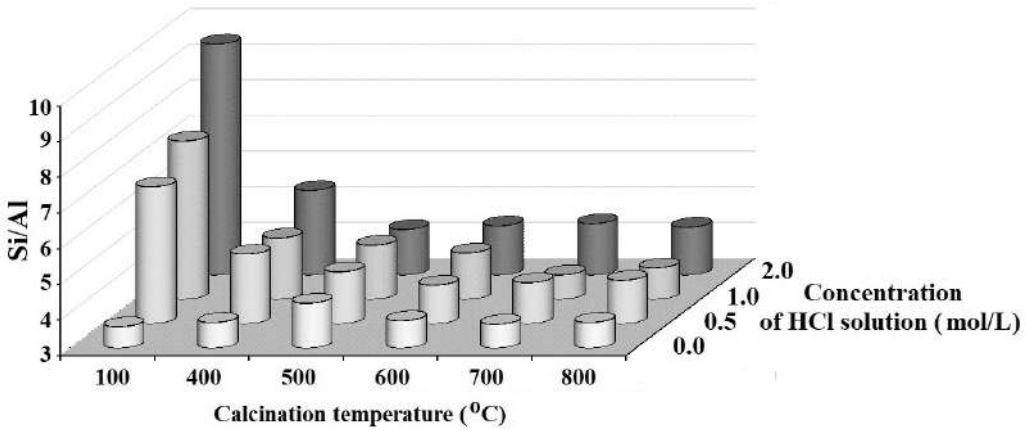

Fig. 12. The Si/Al molar ratio calculated from XR-ED spectra in samples calcined at different temperatures and treated with HCl solutions of various concentrations

Thus, heat treatment does not lead to significant changes in systems of micropores and mesopores, but causes significant structural changes in heulandite. According to measured changes in the Si/Al molar ratio in samples subjected to calcination and then treated with hydrochloric acid solutions (see Fig. 12), such pre-heat treatment significantly reduces the degree of dealumination, especially for samples amorphized by high-temperature calcination.

Perhaps these results are not of practical importance, since at an annealing temperature of 600 °C and above, the corresponding samples lose their adsorption properties, but the structure and properties of the calcined and acid-treated samples require further study and consideration.

CONCLUSIONS

Acid treatment leads to significant dealumination and decationization of heulandite-containing tuff from the Tedzami-Dzegvi deposit, Eastern Georgia, without amorphization, sharply increases the surface area and volume of micropores available for large molecules, and causes changes in the mesoporous system, leading to the prevalence of pores with a diameter up to 4 nm. Heat treatment causes dehydration continuing up to 800 °C, amorphization starting at 200 °C, formation of wairakite at 500 °C, and does not lead to significant changes in pore systems. Heat treatment increases the acid resistance of heulandite by reducing the degree of dealumination after the sample is treated with hydrochloric acid solution. The results obtained show the possibilities of obtaining effective molecular sieves, adsorbents and ion exchangers by modifying natural heulandite.

ACKNOWLEDGEMENT

The authors express their gratitude to the International Science and Technology Center (ISTC) supported this work under the project GE-2506 “Scientific substantiation of the possibility of creating new bactericidal zeolite filter materials for purification-decontamination of water from various sources”.

Кислотна та термічна обробка природного гейландиту

В.Г. Ціцішвілі, Н.М. Долаберідзе, М.О. Ніжарадзе, Н.А. Мірдзвелі, З.С. Амірідзе, Б.Т. Хуцишвілі

Національна академія наук Грузії
пр. Руставелі, 52, Тбілісі, 0108, Грузія, v.tsitsishvili@gmail.com
Інститут фізичної та органічної хімії ім. П. Мелікішвілі Тбіліського державного університету
вул. Г. Політковської, 31, Тбілісі, 0186, Грузія

Кислотна обробка природних цеолітів вважається ефективним методом «поліпшення» їхньої структури та властивостей, серед яких особливе місце припадає термостійкість, особливо для каталітичного застосування цеолітів. Досліджено вплив розчинів соляної кислоти концентрацією до 2 mol/L та прожарювання при температурах до 1100 °C на структуру та властивості гейландитвмісного туфу грузинського родовища Дзегві-Тедзамі, відібраного для створення нових бактерицидних цеолітових фільтрувальних матеріалів для очищення та знезараження води з різних джерел, досліджували рентгенівськими енергетичними дисперсійними спектрами, дифрактограмами та термічним аналізом, а також адсорбційними методами води, бензолу та азоту. Встановлено, що кисле середовище призводить до значного деалюмінування (молярне відношення Si/Al зростає з 3.6 до 9.5) та декатіонізації (сумарний заряд іонів металу на атом Al зменшується з 1 до 0.68) зразка; розчини соляної кислоти не призводять до аморфізації мікропористої кристалічної структури цеоліту, а поступово розчиняють її. В результаті кислотної обробки також різко збільшується об’єм мікропор, доступних для великих молекул (від ≈ 7 до 80–90 мм^3/г) і площа поверхні (від ≈ 13 до 120–175 м^2/г), а також зміни мезопористої системи, що призводять до переважання пор діаметром до 4 нм. Нагрівання гейландиту призводить до ступінчастої дегідратації, що триває до ≈ 800 °C, аморфізації, починаючи з ≈ 250 °C, і структурних змін: перехід у фазу метастабільного гейландиту B при ≈ 340 °C не фіксується, але при ≈ 500 °C утворюється вайракіт ($Ca(Al_2Si_4O_{12})\cdot 2H_2O$), при температурах вище ≈ 1000 °C аморфний алюмосилікат містить кристалічні включення кристобаліту (поліморф SiO_2), α-кварцу, альбіту ($Na(AlSi_3O_8)$, гематиту (Fe_2O_3) та магнетиту ($FeO\cdot Fe_2O_3$); викликані нагріванням зміни мікро- та мезопорових систем незначні. Показано також, що термообробка підвищує

кислотостійкість гейландиту, що виражається в зниженні ступеня деалюмінування після кислотної обробки прожарених зразків. Таким чином, кислотна і термічна обробка гейландиту дають змогу отримати матеріали з різними сорбційними та іонообмінними властивостями.

***Ключові слова**: гейландит, деалюмінування, декатіонізація, дегідратація, аморфізація*

REFERENCES

1. Vasconcelos A.A., Len T., de Oliveira A.dN., da Costa A.A.F., da Silva Souza A.R., da Costa C.E.F., Luque R., da Rocha Filho G.N., Noronha R.C.R., do Nascimento L.A.S. Zeolites: a theoretical and practical approach with uses in (bio)chemical processes. *Appl. Sci*. 2023. **13**(3): 1897.
2. de Magalhães L.F., da Silva G.R., Peres A.E.C. Zeolite application in wastewater treatment. *Ads. Sci. Technol*. 2022. **2022**: 4544104.
3. Andrunik M., Bajda T. Removal of pesticides from waters by adsorption: comparison between synthetic zeolites and mesoporous silica materials. A review. *Materials*. 2021. **14**(13): 3532.
4. Grela A., Kuc J., Bajda T. A review of the application of zeolites and mesoporous silica materials in the removal of non-steroidal anti-flammatory drugs and antibiotics from water. *Materials*. 2021. **14**(17): 4994.
5. Wang S., Peng Y. Natural zeolites as effective adsorbents in water and wastewater treatment. *Chem. Eng. J*. 2010. **156**(1): 1.
6. Çakicioğlu-Özkan F., Becer M. Effect of the acid type on the natural zeolite structure. *J. Turk. Chem. Soc. Sect. A Chem.* 2019. **2**(2): 69.
7. Rozić M., Cerjan-Stefanović S., Kurajica S., Maeefat M.R., Margeta K., Farkas A. Decationization and dealumination of clinoptilolite tuff and ammonium exchange on acid-modified tuff. *J. Colloid Interface Sci*. 2005. **284**(1): 48.
8. Cakicioglu-Ozkan F., Ulku S. The effect of HCl treatment on water vapor adsorption characteristics of clinoptilolite rich natural zeolite. *Microporous Mesoporous Mater.* 2005. **77**(1): 47.
9. Tsitsishvili V., Panayotova M., Miyamoto M., Dolaberidze N., Mirdzveli N., Nijaradze M., Amiridze Z., Klarjeishvili N., Khutsishvili B., Dzhakipbekova N., Harutyunyan L. Characterization of Georgian, Kazakh and Armenian natural heulandite-clinoptilolites. *Bulletin of The Georgian National Academy of Sciences.* 2022. **16**(4): 115.
10. Tsitsishvili V., Machaladze T., Dolaberidze N., Nijaradze M., Mirdzveli N., Djakipbekova N., Harutyunyan L. Dehydration and structural transformations during thermal treatment of Georgian, Kazakhstani and Armenian natural heulandite-clinoptilolites. *Scientific collection InterConf*. 2022. **136**: 356.
11. Tsitsishvili V., Dolaberidze N., Mirdzveli N., Nijaradze M., Dzhakipbekova N., Harutyunyan L., Amiridze Z,, Khutsishvili B. Acid treatment of Georgian, Kazakhstani and Armenian natural heulandite-clinoptilolites. *Scientific collection InterConf*. 2022. **138**: 363.
12. Tsitsishvili V., Dolaberidze N., Mirdzveli N., Nijaradze M., Dzhakipbekova N., Harutyunyan L., Amiridze Z., Khutsishvili B. Acid treatment of Georgian, Kazakhstani and Armenian natural heulandite-clinoptilolites. II. Adsorption and porous structure. *Scientific collection InterConf*+. 2023. **31**(147): 483.
13. Tsitsishvili V., Dolaberidze N., Mirdzveli N., Nijaradze M., Dzhakipbekova N., Harutyunyan L., Amiridze Z., Khutsishvili B. Thermal treatment of Georgian, Kazakhstani and Armenian natural heulandite-clinoptilolites. *Scientific collection InterConf*+. 2023. **29**(139): 242.
14. Tsitsishvili V., Panayotova M., Mirdzveli N., Dzhakipbekova N., Panayotov V., Dolaberidze N., Nijaradze M. Acid resistance and ion-exchange capacity of natural mixtures of heulandite and chabazite. *Minerals*. 2023. **13**(3): 364.
15. Mumpton F.A. Clinoptilolite redefined. *Am. Mineral*. 1960. **45**: 351.
16. Koizumi M. The differential thermal analysis curves and the dehydration curves of zeolites. *Mineralogical J*. 1953. **1**(1): 36.
17. Pechar F., Rykl D. Study of the thermal stability of the natural zeolite heulandite. *Chem. Pap*. 1985. **39**(3): 369.
18. Dang L., Le S., Lobo R., Pham T. Hydrothermal synthesis of alkali-free chabazite zeolites. *J. Porous Mater*. 2020. **27**: 1481.
19. Lide D.R. *CRC Handbook of Chemistry and Physics*. *81st Edition*. (Boca Raton FL: CRC Press LLC, 2000).
20. Olson D.H., Haag W.O., Borghard W.S. Use of water as a probe of zeolitic properties: interaction of water with HZSM-5. *Microporous Mesoporous Mater.* 2000. **35/36**: 435.

21. Brunauer S., Deming L., Deming W., Teller E. On a theory of the van der Waals adsorption of gases. *J. Am. Chem. Soc*. 1940. **62**(7): 1723.
22. Sing K.S.W., Everett D.H., Haul R.A.W., Moscou L., Pierotti R.A., Rouquérol J., Siemieniewska T. Reporting physisorption data for gas/solid systems with special reference to the determination of surface area and porosity. *Pure Appl. Chem*. 1985. **57**(4): 603.
23. Brunauer S., Emmett P.H., Teller E. Adsorption of gases in multimolecular layers. *J. Am. Chem. Soc*. 1938. **60**(2): 309.
24. Barrett E.P., Joyner L.G., Halenda P.P. The determination of pore volume and area distributions in porous substances. I. Computations from nitrogen isotherms. *J. Am. Chem. Soc*. 1951. **73**(1): 373.
25. Halsey G.D. Physical adsorption on non-uniform surfaces. *J. Chem. Phys*. 1948. **16**: 931.
26. Faass G.S. Correlation of gas adsorption, mercury intrusion, and electron microscopy pore property data for porous glasses. Thesis, Chemical Engineering. (Georgia Institute of Technology, US, 1981). http://hdl.handle.net/1853/32965
27. Akimkhan A.M. Structural and Ion-Exchange Properties of Natural Zeolite. In: *Ion Exchange Technologies*. (London: IntechOpen, 2012).
28. Silva M., Lecus A., Lin Y.T., Corrao J. Tailoring natural zeolites by acid treatments. *J. Mater. Sci. Chem. Eng.* 2019. **7**(2): 26.

Received 21.06.2023, accepted 27.11.2023